Visualizing the subcellular localization of RHOB-GTP and GTPase-Effector complexes using a split-GFP/nanobody labelling assay

Sebastian Castillo, Rémi Gence, Delphine Pagan, Faten Koraïchi, Catherine Bouchenot, Benoit J Pons, Betty Boëlle, Aurélien Olichon, Isabelle Lajoie-Mazenc, Gilles Favre, et al.

European Journal of Cell Biology 102 (2023) 151355

Contents lists available at ScienceDirect

European Journal of Cell Biology

journal homepage: www.elsevier.com/locate/ejcb

Visualizing the subcellular localization of RHOB-GTP and GTPase-Effector complexes using a split-GFP/nanobody labelling assay

Sebastian Castillo [a], Rémi Gence [a], Delphine Pagan [a], Faten Koraïchi [a], Catherine Bouchenot [b], Benoit J. Pons [c], Betty Boëlle [a], Aurélien Olichon [d], Isabelle Lajoie-Mazenc [a], Gilles Favre [a], Jean-Denis Pédelacq [e], Stéphanie Cabantous [a,*]

[a] Centre de Recherche en Cancérologie de Toulouse (CRCT), INSERM, Université de Toulouse, UPS, CNRS, 31037 Toulouse, France
[b] Univ. Grenoble Alpes, CNRS, LIPhy, F-38000 Grenoble, France
[c] Environment and Sustainability Institute, Biosciences, University of Exeter, Penryn TR10 9FE, United Kingdom
[d] Université de la Réunion, INSERM, UMR 1188 Diabète Athérothrombose Thérapies Réunion Océan Indien (DéTROI), 97410 Saint-Pierre, La Réunion, France
[e] Institut de Pharmacologie et de Biologie Structurale (IPBS), Université de Toulouse, CNRS, Université Toulouse III - Paul Sabatier (UPS), Toulouse, France

ARTICLE INFO

Keywords:
Small GTPase
RHOB
Split-GFP
Nanobody
Endosome
Localization

ABSTRACT

Small GTPases are highly regulated proteins that control essential signaling pathways through the activity of their effector proteins. Among the RHOA subfamily, RHOB regulates peculiar functions that could be associated with the control of the endocytic trafficking of signaling proteins. Here, we used an optimized assay based on tripartite split-GFP complementation to localize GTPase-effector complexes with high-resolution. The detection of RHOB interaction with the Rhotekin Rho binding domain (RBD) that specifically recognizes the active GTP-bound GTPase, is performed *in vitro* by the concomitant addition of recombinant GFP1–9 and a GFP nanobody. Analysis of RHOB-RBD complexes localization profiles combined with immunostaining and live cell imaging indicated a serum-dependent reorganization of the endosomal and membrane pool of active RHOB. We further applied this technology to the detection of RHO-effector complexes that highlighted their subcellular localization with high resolution among the different cellular compartments.

1. Introduction

Small GTPases are molecular switches that alternate between an inactive form bound to GDP and an active form bound to GTP. Once activated, they specifically interact with effectors to stimulate downstream signaling pathways. Due to the high sequence similarities that exist within GTPases of the same subfamily (Smithers and Overduin, 2016), they often share a common set of effector proteins. This is especially true for the RHO isoforms, considering that most of RHOA/C effector proteins discovered to date are also shared by RHOB (Wheeler and Ridley, 2004). Nevertheless, these three GTPases can achieve distinct cellular functions, which have been largely attributed to their different subcellular localization. Indeed, RHOA regulates actomyosin contractility that is essential for cell migration and localizes mainly to the plasma membrane (PM) and the cytosol (Ridley, 2013). RHOB is a key component of vesicular transport, and has been shown to regulate the trafficking of Epidermal Growth Factor Receptor (EGFR) (Gampel et al., 1999), Platelet-Derived Growth Factor Receptor (PDGFR) (Huang et al., 2007) and the non-receptor tyrosine kinase Src (Sandilands et al., 2004). RHOB is mainly localized in endosomes, from late endosomes and lysosomes (Wherlock et al., 2004) to early endosomes (Rondanino et al., 2007) and at the plasma membrane (Michaelson et al., 2001; Valero et al., 2010; Wherlock et al., 2004). The specific membrane targeting is conferred by several post-translational lipid modifications in the hypervariable region, at the C-terminus of the protein, where significant differences between the sequences of RHOA and RHOB occur. RHOA is only geranylgeranylated, whereas RHOB contains two palmitoylated cysteine residues next to a prenylation motif (Wang and Sebti, 2005) undergoing geranylgeranyl or farnesyl modifications (Michaelson et al., 2001; Milia et al., 2005; Oeste et al., 2014; Wherlock et al., 2004). Fluorescent proteins fused to the last eight amino acids (CINCCKVL) of RHOB carrying the lipid post-translational modifications mimic RHOB localization at endolysosomal compartments (Oeste et al., 2014). It has also been reported that RHOA-(1−180)/ RHOB-(181−196) chimera, but

* Corresponding author.
E-mail address: stephanie.cabantous@inserm.fr (S. Cabantous).

https://doi.org/10.1016/j.ejcb.2023.151355
Received 23 March 2023; Received in revised form 4 August 2023; Accepted 20 August 2023
Available online 21 August 2023

not wild-type RHOA, phenocopies the ability of RHOB to inhibit tumor growth and induces apoptosis (Wang and Sebti, 2005). Furthermore, the function of small GTPase is also tightly regulated by the subcellular localization of regulators and effector proteins (Ellenbroek and Collard, 2007). Therefore, analyzing the cellular distribution of small GTPases in complex with their binding partners is essential to provide a better understanding of their activation mechanisms.

Common approaches to localize small GTPases use N-terminally fused fluorescent proteins that allow high-resolution imaging and multiplexing for combined immunofluorescence analysis (Arnette et al., 2016; Gong et al., 2018; Marcos-Ramiro et al., 2016; Michaelson et al., 2001). Nevertheless, these approaches provide limited information on the activation state of GTPases and cannot distinguish the fraction of GTPase that is bound to effector proteins from the total amount of GTPase expressed. Other live-cell methods, such as Fluorescence Resonance Energy Transfer (FRET) biosensors, have been successfully used to report the dynamic distribution of active GTPases (Pertz et al., 2006; Yoshizaki et al., 2003) and have been adapted to study the spatiotemporal activation of RHOB in endothelial cells (Reinhard et al., 2016). These probes display a poor spatial resolution for addressing protein complexes localization and cannot be easily adapted to multiple targets. Another class of protein-protein interaction sensors consists of split complementation assays that reconstitute the reporter protein function when proteins of interest (POI) associate (Wehr and Rossner, 2016). Tripartite split fluorescent protein complementation presents the advantage of using small fusion tags (20 amino-acids) that have proven not to perturb protein folding and localization (Cabantous et al., 2013; Keller et al., 2022; Koraïchi et al., 2018). Unlike bimolecular complementation systems that spontaneously associate upon interaction, the tripartite split-GFP system relies on a two-step process involving protein interaction first and subsequent reconstitution of the GFP, resulting in lower fluorescence background. Bait and prey proteins are fused to strands β-10 (GFP10) and β-11 (GFP11), while detection of the nearby GFP10 and GFP11 tags is achieved by the large complementary detector fragment (strands β1–9 or GFP1–9), which leads to GFP fluorescence (Cabantous et al., 2013). We previously applied this technology to monitor the interactions of RHOB with the Rho binding domain (RBD) of rhotekin in live cells (triSFP RHOBact). We demonstrated that the output GFP fluorescence correlates with the GTPase-effector interaction, which involves the active GTP-bound form of the GTPase. This activation is triggered by GEF (Koraïchi et al., 2018). However, in such models, the detector fragment GFP1–9 is constitutively expressed in the cell and, when protein-protein interactions (PPI) occur, RHOB/RBD complexes accumulate and may degrade over time depending on the stability of the tagged proteins. Therefore, visualization of GFP signals may reflect the formation of intact RHOB/RBD complexes that may have occurred prior to imaging. To circumvent this drawback, we developed a protocol that consists in co-expressing GFP10 and GFP11 fusion proteins in live cells, and detecting protein complexes after a fixation/permeabilization step using purified recombinant GFP1–9 (Fig. 1A). In this scheme, the observed GFP fluorescence accurately reports the localization of protein complexes upon cell fixation. Because detection was less efficient with GFP1–9 alone, we used a recombinant GFP nanobody to enhance fluorescence signals. Using RHOB/RBD interactions as a study model, a comparison of the live cell approach with the *in vitro* labelling assay showed a differential serum-dependent distribution of endosomal and plasma membrane pools of active RHOB. Using time-lapse imaging and photobleaching experiments, we demonstrated that the accumulation of active RHOB at the plasma membrane originates from trafficking of endosomal active RHOB towards the cell surface. We further applied this procedure to the detection of full-length RHOA and RHOB effector protein complexes that showed a redistribution of effectors to the site-specific localization of RHOA and RHOB.

2. Results

2.1. Improvement of GFP1-9 complementation for in situ protein complexes labelling

In light of previous results that demonstrated a "booster" effect of a GFP nanobody on the tripartite split-GFP complementation (Koraïchi et al., 2018), we used this concept to improve split-GFP fluorescence for *in situ* protein complexes labelling. To test this approach, we first set up an *in vitro* complementation assay using recombinant coiled-coils domains (GFP10-K/E-GFP11) with different ratios of 0.1 mg/mL solutions of purified recombinant GFP1–9 (GFP1–9r) and anti-GFP VHH (VHHr) (Supp. Fig. 1A, left graph). Our results indicated that the GFP nanobody significantly improves the efficiency of split-GFP reconstitution with increasing VHHr to GFP1–9r ratios. Importantly, GFP1–9 autofluorescence was not increased when both GFP1–9r and the VHHr were incubated together (Supp. Fig. 1A, right graph). To validate the benefits of VHHr for protein complex labelling and fluorescence microscopy imaging, we used the FRB/FKBP rapamycin complex inducible system (Banaszynski et al., 2005). We coexpressed GFP10-FRB and FKBP-GFP11 following transfection in MRC5 fibroblasts that were treated or not with 100 nM rapamycin for 24 h. We next performed a split-GFP complementation assay *in vitro* on fixed and permeabilized cells by adding purified recombinant GFP1–9 or a combination of GFP1–9r/VHHr to a 4:1 vol ratio (see methods) that was chosen to provide sufficient fluorescent signal compared to GFP1–9r alone. Fluorescence complementation was only detected in cells treated with rapamycin, as expected (Fig. 1B). In the GFP1–9r/VHHr condition, the number of positive cells was increased by a factor 2 but their relative fluorescence intensities did not vary significantly compared to GFP1–9r alone (Fig. 1B). These results indicate that the anti-GFP nanobody increases the maturation of GFP upon split-GFP complementation in binding conditions (+RAP) while complementation is not significant in non-binding conditions (-RAP). Next, we used this approach to visualize the localization of active GTPases. We modified the initial model developed by Koraïchi et al. (Koraïchi et al., 2018) by engineering two doxycycline-inducible vectors. These vectors include a fusion of the RHO GTPase with a N-terminal GFP10 tag, followed by an IRES-BFP tag cassette in one vector, and the RBD of rhotekin preceeding an IRES-mCherry reporter in the other (Supp. Fig. 1B). MRC5 Tet-On fibroblasts stably expressing these constructs were induced with doxycycline and were subsequently fixed/permeabilized before labelling with GFP1–9r alone or for GFP1–9r/VHHr. We assessed the kinetic of detection of GFP fluorescence during the labelling procedure. The minimum time for optimal detection was 4 h at room temperature using a GFP1–9r/VHHr ratio of 4:1 (Fig. 1C, Supp. Fig. 1C). High-content imaging measurements indicated that both the number of positive cells and their fluorescence increased, confirming the real benefit of combining VHHr with GFP1–9r labelling at low expression levels (Fig. 1C). According to the GFP fluorescence quantification, cellular structures showed brighter fluorescence in the presence of VHHr. Similarly, we could detect a similar fluorescence boosting effect using a commercial VHHr (ChromoTek®) under the same conditions (Supp. Fig. 1D). The efficiency of GFP complementation using recombinant GFP1–9 purified either by the immobilized metal affinity chromatography (IMAC) followed by size exclusion chromatography (SEC), or only by IMAC using the batch method, was found to be similar in terms of the number of GFP-positive cells and GFP fluorescence (Supp. Fig. 1E). Therefore, this method using recombinant purified GFP1–9 can be easily setup with basic laboratory equipment and using commercial recombinant VHH.

2.2. Localization of active RHOB in serum-starved and serum-stimulated cells

Apart from FRET biosensors (Reinhard et al., 2016), current studies

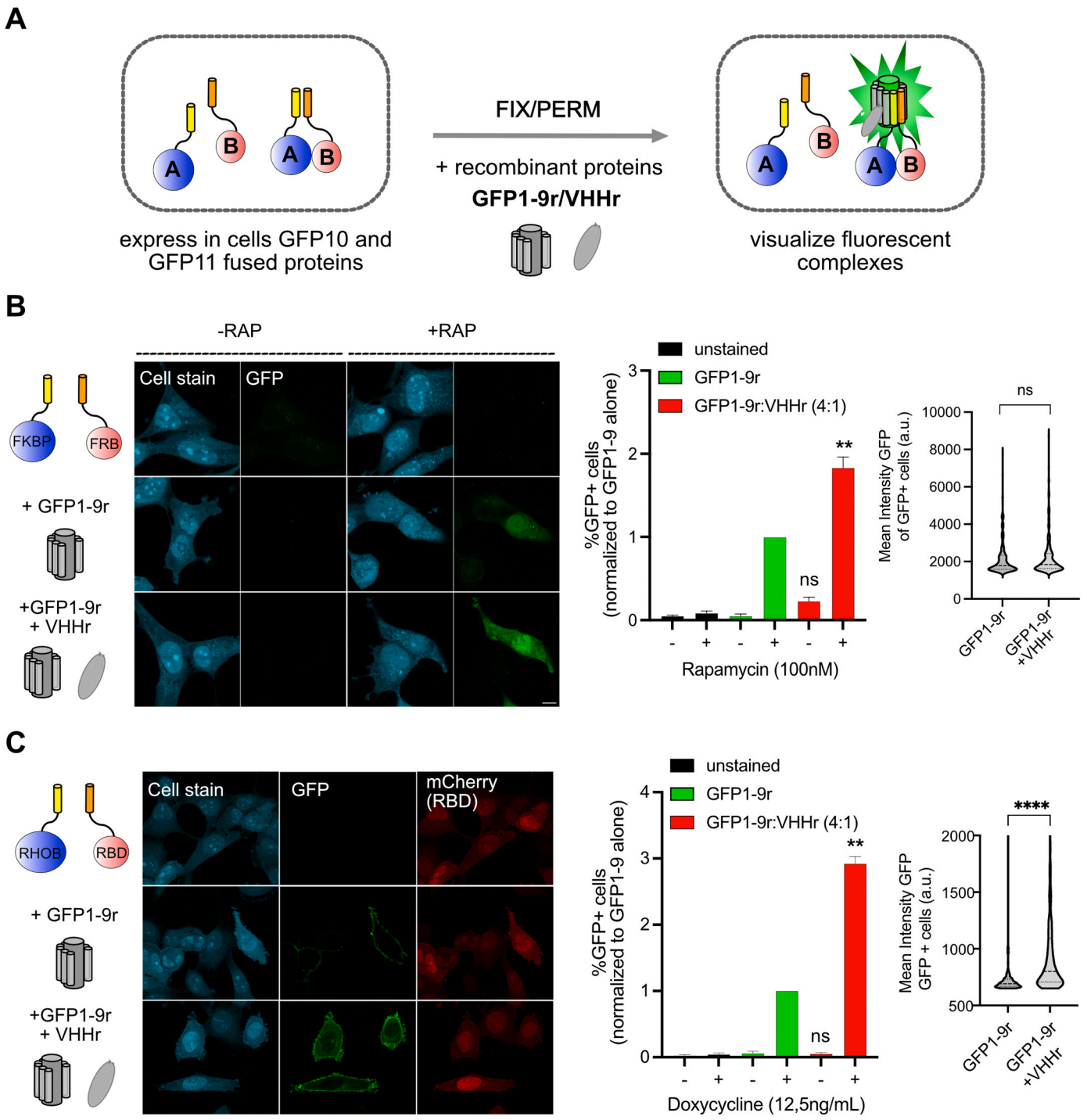

Fig. 1. Detection of protein complexes using tripartite split-GFP *in vitro* labelling. (A) Scheme of the tripartite split-GFP labelling assay. Protein A is fused to strand β-10 and Protein B to strand β-11. After protein expression, cells are fixed/permeabilized and a solution of recombinant GFP 1–9 (GFP1–9r) with a anti-GFP nanobody (VHHr) is added and incubated for 4 h at room temperature. Following *in vitro* split-GFP complementation, only A/B protein complexes are visualized. (B) Analysis of the *in vitro* reconstitution of GFP upon coexpression of GFP10-FRB and FKBP-GFP11 fusions in the presence (+RAP) or absence (-RAP) of rapamycin, followed by *in vitro* labelling with GFP1–9r or GFP1–9r/VHHr. Unstained MRC5 cells are used as background cell fluorescence control. Left: Representative confocal microscopy images of the samples. Middle: Quantification of the GFP positive cells number relative to the total cell population (cell stain) (% GFP+ cells, normalized to the % GFP+ cells detected with GFP1–9 alone, n = 3 independent experiments, mean ± SEM). Student's t-test between GFP1–9r/VHHr and GFP1–9r, * *P < 0.01. Right: The mean intensity of the GFP positive cells is shown next (representative experiment; n = 224 cells (GFP1–9r) n = 249 cells (GFP1–9r/ VHHr); Student's t-test ns= non-significant). (C) Left: Representative confocal microscopy images of the samples. Middle: Quantification of GFP following GFP1–9 *in vitro* labelling using a stable cell model RHOB/RBD. MRC5 cells were induced with doxycycline for 24 h, then stained with GFP1–9r or GFP1–9r/VHHr. Quantification of GFP positive cells (normalized to the % GFP+ cells detected with GFP1–9 alone; n = 3 independent experiments, mean ± SEM). between GFP1–9r/VHHr and GFP1–9r, Student's t-test * *P < 0.01. Right: GFP mean fluorescence intensity of the GFP population (representative experiment, n = 395 cells (GFP1–9r) n = 1160 cells (GFP1–9r/VHHr); Student's t-test * ** *P < 0.001).

on RHOB trafficking uses either GFP fusions of active mutants to localize RHOB (Arnette et al., 2016; Gong et al., 2018; Marcos-Ramiro et al., 2016; Michaelson et al., 2001). So far only pulldown assays or colocalization analyses have been used to technically show the binding of RHO to their effectors. In that respect, Rhotekin Rho binding domain (RBD) serves as a standard recognition domain to pull down the active GTP-bound conformation of RHO GTPases (Reid et al., 1996). To analyze specifically the localization of its active form (GTP-bound) in single cells, we monitored the interaction between wild-type RHOB and the RBD domain (Supp. Fig. 1B). Twenty-four hours after doxycycline induction, we fixed the cells and performed a GFP1–9r/VHHr labelling procedure, to allow the imaging of reconstituted GFP that reports RHOB/RBD interaction. Furthermore, we added an immunofluorescence staining step that uses an antibody specific to GFP10 (rabbit immune serum) (Koraïchi et al., 2018) to visualize the subcellular localization of expressed GFP10-RHOB (Fig. 2). Immunofluorescence on MRC5 cells expressing GFP10-RHOB indicated a total overlap between anti-GFP10 and anti-RHOB immunostainings (Supp. Fig. 2A). In contrast, immunostaining of cells expressing full length tripartite GFPr failed (Supp. Fig. 2B), which demonstrates that the anti-GFP10 antibody reveals only the free unbound GFP10-tagged protein that is not engaged within the GFP barrel.

We first assessed the effect of serum onto the localization of activated RHOB by expressing GFP10-RHOB/RBD-GFP11 either in serum-starved conditions (0.1% BSA) or in serum-enriched medium (10% FBS). In these conditions, we observed using GST-RBD pulldown assay, an increase of active RHOB between starved and serum stimulated cells (Supp. Fig. 2C). Representative confocal microscopy images of serum-starved cells revealed split-GFP fluorescence signals in intracellular vesicles, with a discrete localization at the plasma membrane (Fig. 2A, a). In contrast, cells cultivated in serum-enriched medium showed bright split-GFP fluorescence at the plasma membrane and weak vesicular GFP staining (Fig. 2A, b). Merge of split-GFP and GFP10 confocal images revealed regions where GFP10-RHOB was expressed but not bound to RBD (Fig. 2A, a-b). Quantification indicated that the ratio of GFP fluorescence in the vesicular region to the total cell fluorescence (Supp. Fig. 2D) was decreased by a factor 2 in serum-enriched compared to serum-starved conditions (Fig. 2A top left graph). This is in agreement with the localization of expressed RHOB (GFP10-RHOB) that localized preferentially in vesicular region in serum-starved conditions compared to serum-enriched conditions cells (Supp. Fig. 2E). We next compared these results with the split-GFP cell model in which GFP10-RHOB/RBD-GFP11 and the GFP1–9/VHH are coexpressed (triSFP RHOBact) (Koraïchi et al., 2018). Serum stimulation induced a profile close to what was observed using recombinant GFP1–9 labelling, resulting in a decrease by a factor of 3 of the vesicular/total GFP fluorescence compared to serum-starved conditions (Fig. 2A c-d bottom left graph). In accordance with previous results and the biochemical GST-RBD assay (Supp. Fig. 2C), the overall GFP fluorescence increased after serum stimulation in the triSFP RHOBact cell model (Koraïchi et al., 2018) and was reproducible using the recombinant GFP1–9 labelling (Fig. 2A, right graphs).

Since the localization of RHOB/RBD increased at the plasma membrane upon serum stimulation, we investigated whether the localization of GFP at the plasma membrane was linked to RHOB activation. We therefore treated the triSFP RHOBact biosensor cells with the cell permeable C3 exoenzyme Rho inhibitor (TAT-C3) (Aktories et al., 2004; Sahai and Olson, 2006) for 24 h in the presence of serum (FBS 10%) and performed an anti-GFP10 immunostaining to visualize expressed GFP10-RHOB. Our results revealed a loss of the split-GFP labelling in both the plasma membrane and in vesicles of TAT-C3-treated cells, correlating with the absence of RHOB activation in the presence of the inhibitor (Fig. 2B). This was accompanied with a predominant staining of GFP10-RHOB in endosomes in C3-treated cells in contrast to control cells that showed GFP10-RHOB localization both at the plasma membrane and in endosomes. These results suggest that in absence of activation, RHOB do not localize to the plasma membrane. One hypothesis is that the accumulation of active RHOB at the plasma membrane depends on its endosomal activation. To confirm this, we performed FLIP (Nissim-Rafinia and Meshorer, 2011) experiments on the triSFP RHOBact biosensor cell model by quenching the endosomal pool while measuring the GFP fluorescence in a region from the plasma membrane. Repetitive photobleaching of an area centered on the endosomal pool of active RHOB gradually decreased the fluorescence signal at the plasma membrane (Fig. 2**C**, **Supp. Video file**). Nine repetitive cycles of photobleaching resulted in a decrease of 74% of the initial fluorescence intensity at the plasma membrane within 25 min. Control measurements from an adjacent non-irradiated cell indicated as expected no variation of the fluorescence intensity of the neighbor cell (Fig. 2**C**, reference cell). Altogether, our results show that the signal observed at the plasma membrane in serum stimulated conditions originates from the trafficking of endosomal RHOB towards the membrane.

Supplementary material related to this article can be found online at doi:10.1016/j.ejcb.2023.151355.

To characterize which endosomal pool is relocalized upon serum stimulation, we expressed the RHOB/RBD reporter in cells under either serum-starved conditions (0.1% BSA) or serum-enriched medium (10% FBS). Subsequently, we fixed the cells for GFP1–9r/VHHr staining followed by immunostaining with several endosomal markers for which RHOB has been shown to colocalize: EEA1 (Rondanino et al., 2007) Rab7 (Marcos-Ramiro et al., 2016) LAMP1 (Wherlock et al., 2004) and Rab11 (Gong et al., 2018; Samuelsson et al., 2017) (Fig. 3A). Analysis of Manders' overlap coefficient indicated a preferential colocalization of the reconstituted GFP with Rab7 late endosomal marker (0.41) and the Early Endosome-Associated protein 1 EEA1 (0.32), followed by the Lysosomal Associated Protein 1 (LAMP1) (0.12) and the recycling endosome Rab11 (0.157) (Fig. 3B) in serum starved conditions. In serum stimulated conditions, we quantified a significant decrease of GFP colocalization with early and late endosomal markers (EEA1, Rab7, LAMP1) (Fig. 3B) In contrast, colocalization of RHOB/RBD complexes with Rab11 was increased in serum stimulated cells, suggesting that RHOB trafficking towards the cell surface transits partially through this compartment. As a comparison, the decrease of endosomal staining of GFPr (RHOB/RBD) in serum stimulated conditions was more pronounced in the triSFP RHOB cell model than in the *in vitro* GFP1–9 assay (Supp. Fig. 3A). Notably, we did not notify changes in colocalization between free GFP10-RHOB and endosomes in starved and stimulated conditions (Supp. Fig. 3B), suggesting that the loss of GFP in endosomes results from the trafficking of activated RHOB molecules (ie RHOB/RBD) as demonstrated in Fig. 2C.

Altogether, our results show that in MRC5 fibroblasts, RHOB/RBD complexes localize mainly in EEA1 and Rab7 endosomal compartments markers. In serum-stimulated conditions, colocalization with these markers decreases, and RHOB/RBD partially traffics through the recycling endosome Rab11 to reach the plasma membrane (Fig. 3C).

2.3. Localization of RHO-effector complexes

To further exploit our strategy for detecting protein complexes and their localization in the context of small GTPase signaling, we investigated the interaction of RHOA/B GTPases with several known effector proteins. Effector proteins comprise a large panel of signaling molecules such as protein kinases that bind active GTP-bound conformation of small GTPases (Bishop and Hall, 2000). Multiple interaction scenarios involving GTPases are possible as one effector can bind several GTPases (Fujisawa et al., 1998). To evaluate whether the split-GFP assay could corroborate published observations and be extended to multiple effectors, we selected three Rho effectors that carry the class I Rho binding motif PRK1, rhotekin (RTKN) and rhophilin (RHPN) (Reid et al., 1996). First, we addressed the question of the localization of the effector itself by transfecting MRC5_Tet-On_GFP10-RHO/effector-GFP11 cells with

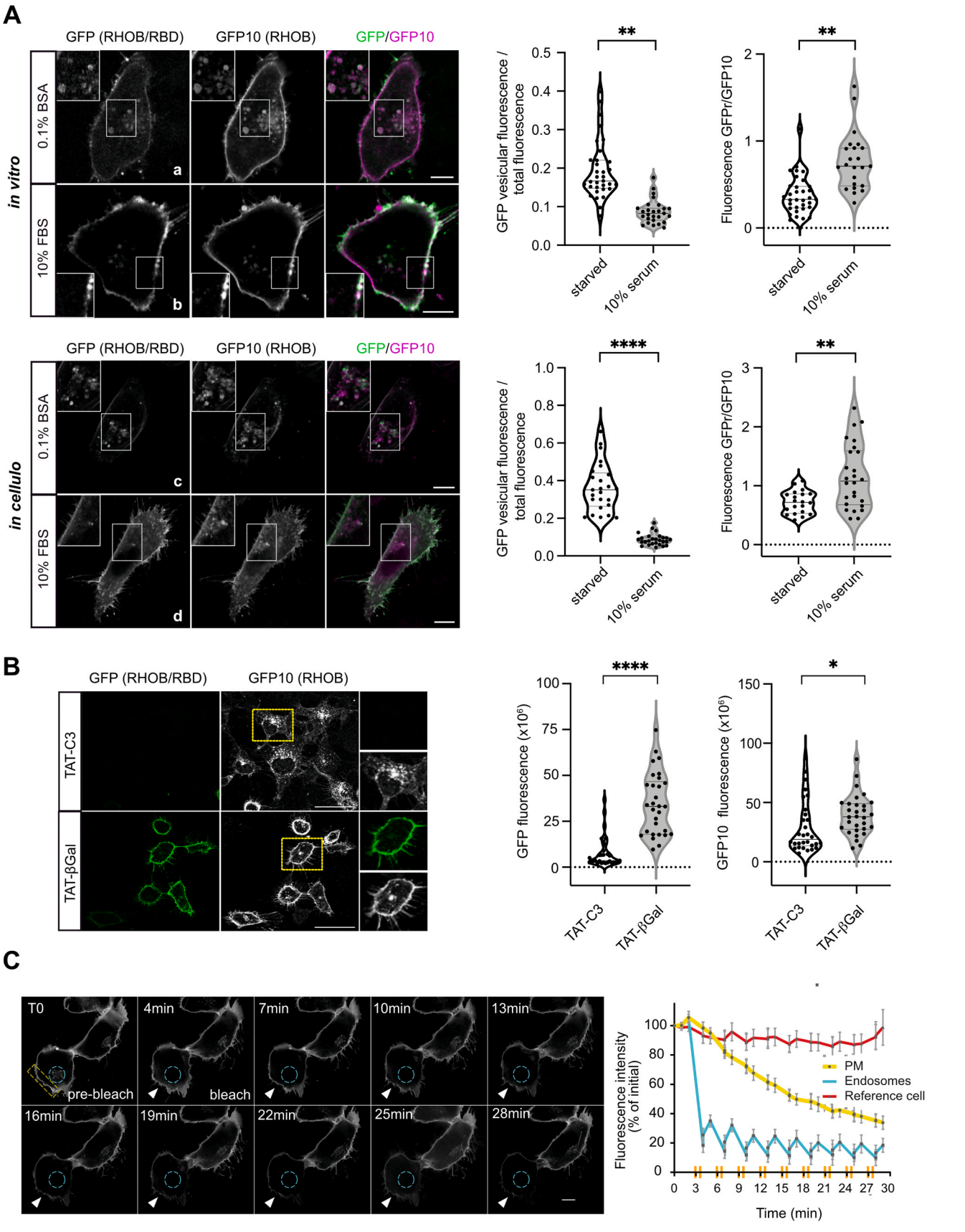

(caption on next page)

Fig. 2. Localization of RHOB/RBD in starved and serum-stimulated cells. (A) Representative confocal images of RHOB/RBD interaction (GFP) and total expressed RHOB revealed with anti-GFP10 antibody (GFP10-RHOB) after 24 h expression in serum-free medium (0.1% BSA) or in serum-enriched medium (10% FBS) for the *in vitro* labelling assay (a, b) and the triSFP model (c, d). Scale bars: 10 μm. Violin plots: quantification of vesicular fluorescence/total GFPr fluorescence (left). Mean ± SEM, n = 25–34 cells, Student's t-test * *P < 0.01; * ** *P < 0.001; Mean integrated density of GFP fluorescence normalized with GFP10 fluorescence (right). Mean ± SEM, n = 25–34 cells, Student's t-test * *P < 0.01. (B) Representative confocal images of RHOB triSFP reporter cells treated in serum-enriched medium simultaneously with doxycycline (0.25 μg/mL) and TAT-C3 Rho inhibitor (5 μg/mL) or with TAT-βGal control (5 μg/mL) for 24 h, followed with GFP10 immunofluorescence (GFP10-RHOB). Scale bar: 10 μm (right panel). Violin plots: quantification of whole cell GFP fluorescence and GFP10 fluorescence. Mean ± SEM, n = 30 cells, Student's t-test * ** *P < 0.0001. n = 3 independent experiments. (C) Fluorescence loss in photobleaching (FLIP) measurement in the live cell split-GFP RHOB/RBD model. Representative sequential images of pre-bleach and post-bleach acquisitions of the biosensor fluorescence at indicated time points. The endosomal pool of RHOB/ RBD was photobleached (cyan circled area) every 3 min and the plasma membrane fluorescence (yellow squared area) was measured every minute. Scale bar: 10 μm. Right graph: Quantification of the normalized percentage of fluorescence intensity over acquisition time relative to the initial fluorescence intensity measured at the plasma membrane (yellow plot) and the bleached area (cyan plot). The red line indicates the normalized fluorescence of an unbleached control cell. The orange lines indicate the photobleaching cycles. Data means ± SEM of $n = 19$ cells from 2 independent experiments.

GFP1–10, a self-assembling domain to GFP11 (Cabantous et al., 2005). GFP fluorescence could be measured 24 h after transfection in the absence of RHO expression. Representative confocal images indicated a diffuse cytoplasmic localization for the effector alone in all three conditions (Fig. 4a, b, c), a result previously reported in the literature for PRK1 (Mellor et al., 1998) and Rhophilin (Steuve et al., 2006). We next revealed the localization of the complex after doxycycline induction of RHO expression using the GFP1–9 *in vitro* labelling assay in MRC5 Tet-On fibroblasts that express GFP10-RHOB or GFP10-RHOA and their corresponding effector C-terminally fused to GFP11 (see methods). In parallel, we also analyzed the localization of GFP10-RHO using GFP10 antibody. Both GFP10-RHOB and RHOB-effector complexes (tripartite split-GFP system) were detected mainly at the plasma membrane and in vesicular compartments (Fig. 4Ad, e, f). Mander's coefficient calculations, into the selected vesicular areas, indicated a similar colocalization of GFP in EEA1 endosomes for all effectors (Fig. 4B). Similarly, colocalization of GFP10-RHOB in EEA1 was not affected by effectors coexpression (Fig. 4C). In contrast, quantification of vesicular/total GFP fluorescence normalized to GFP10 signals revealed a significant increase in the vesicular distribution of RHOB/RHPN complex compared with RHOB/RTKN or RHOB/PRK1 (Fig. 4D). Comparison analysis with RHOA indicates a diffuse cytosolic localization of all RHO-effector complexes with a discrete localization at the plasma membrane that correlates with GFP10-RHOA localization (Fig. 4 Ag, h, i). As a negative control, RHOA and RHOB were coexpressed with NADPH Oxidase 1 (NOX1), an effector of RAC1 (Kao et al., 2008) that does not interact with RHOA/B (Supp. Fig. 4A). To identify if there are discrepancies in the detection of the complex localization when the GFP1–9 is constitutively expressed, we co-transfected GFP1–9 and VHH constructs in MRC5_RHO-effector cells (Supp. Fig. 4B). The GFP fluorescence distribution for RHOB-effector complexes was more important at the plasma membrane, which might reflect a differential migration of RHOB towards the plasma membrane, as observed in Fig. 2 with the RBD domain. The localization of RHOA-effector complexes presented a similar pattern compared to *in vitro* labelling assay (Supp. Fig. 4B). Altogether these results indicate that despite sharing the same effectors, RHOA and RHOB effectors complexes possess distinct localizations that are most predominantly dictated by the localization of the GTPase.

2.4. Discussion

This work explores a new field of application of the split-GFP tripartite technology, namely for the localization of protein-protein complexes in eukaryotic cells. This approach uses the fusion of short fragments GFP10 and GFP11 to proteins of interest whose association is detected by the large complementary fragment GFP1–9. Classically, GFP1–9 is constitutively expressed in the cell where it traps protein complexes that form over the time course of the experiment. In this study, we overcome the drawback of the irreversibility of the tripartite split-GFP complementation scheme by performing a direct labelling of protein-protein complexes on fixed and permeabilized cells. The use of a robust and efficient system was highly desirable for improving the efficiency of the labelling with improved spatiotemporal resolution. We have previously shown that the anti-GFP nanobody/ VHH (Kirchhofer et al., 2010) known as "GFP booster" (Chromotek, Germany) binds specifically to the full length GFP and not individual split-GFP fragments (Koraïchi et al., 2018). We now demonstrate that the combination of GFP1–9 with anti-GFP VHH still preserve high signal to background ratios in the case of the *in vitro* labelling assay using recombinant proteins. We also validated this approach to localize PPI involving small GTPases in subcellular compartments such as endosomes and membranes. The cellular localization of RHOB, as previously shown for the endogenous GTPase (Wherlock et al., 2004) or using GFP fusions (Roberts et al., 2008; Valero et al., 2010), was primarily attributed to endosomes and the plasma membrane, yet there is no evidence of the localization of wild-type RHOB in its active GTP-bound form. Herein, we describe for the first time the cellular distribution of the active GTP-bound RHOB through the sensing of RHOB/RBD complexes (Fig. 2). The contribution of anti-GFP10 immunostaining allowed us to decouple the signal of the GTPase alone (GFP10-RHOB) from the one inside the complex. We were able to detect free RHOB at both the vesicles and the plasma membrane, and observed significant differences for RHOB/RBD complexes in the presence of serum where the loss of GFP signal in early and late endosomes is correlated with an enrichment at the plasma membrane. FLIP experiments indicated that the increase of active RHOB at the plasma membrane in serum cultured cells does not originate from activation of the inactive plasma membrane resident pool, but results from recruitment of the activated endosomal RHOB (Fig. 2C).

The membrane localization of RHOB reported in multiple studies (Gampel et al., 1999; Huang et al., 2011, 2007; Lajoie-Mazenc et al., 2008; Mellor et al., 1998), may depend on the balance between F and GG prenylation forms of the GTPase to target the plasma membrane or the endosomes respectively (Milia et al., 2005) and on the plasma membrane-vesicle trafficking of cells, as demonstrated by Gong and colleagues (Gong et al., 2018). Coupling of the biosensor to markers of subcellular compartments revealed that the distribution profile of RHOB/RBD correlates mostly with late and early labeled endosomes under serum starvation conditions (Fig. 3). This suggests that active RHOB primary localizes in the endosomes, and mostly in early and late endosomes, and that stimulation of cell signaling by serum triggers their movement towards the PM. The enrichment of RHOB/RBD with Rab11 in serum stimulated conditions goes along the same line, thus predicting that the trafficking of RHOB towards the cell surface transits through this compartment. Data from the literature converge towards this observation, as shown by Lungu and colleagues who identified the GEF Solo that regulates RHOB activation and endocytic trafficking (Lungu et al., 2023). A regulating kinesin KIF13A of the trafficking of RHOB positive endosomes to the plasma membrane was recently identified to control ameboid migration (Gong et al., 2018). Functions of RHOB at the plasma membrane could be linked to its role in cell migration and adhesion. Indeed, RHOB plays an active role in the control of the dynamic of focal adhesions (Vega et al., 2012), and acts in coordination with Rac1 to form cell protrusions (Huang et al., 2011; Vega et al.,

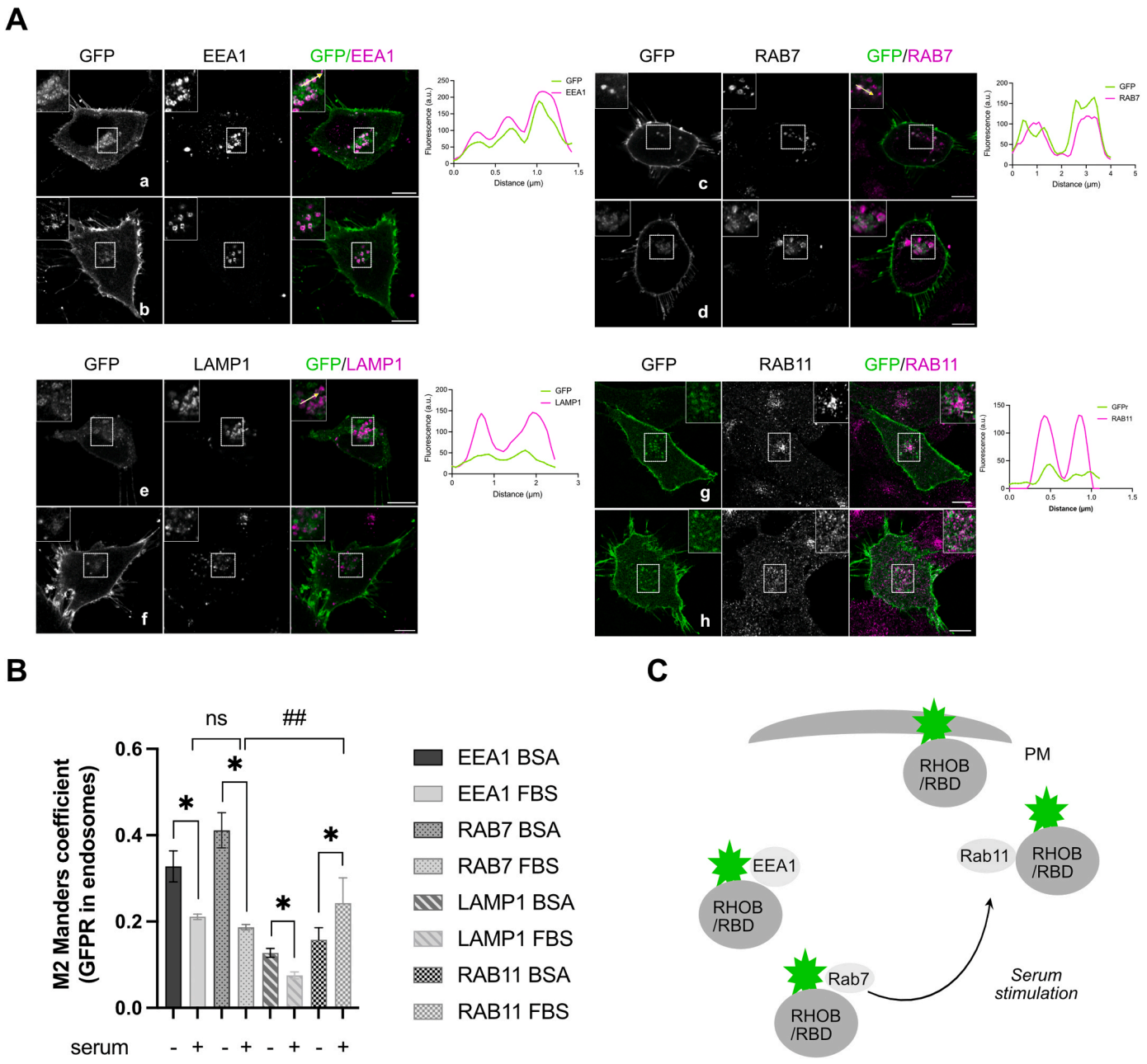

Fig. 3. Colocalization of RHOB/RBD with endosomal markers. (A) Representative images of GFP (green) colocalization with early (EEA1) and late (Rab7) endosomes, lysosomes (LAMP1) and recycling endosome Rab11 (magenta) using the *in vitro* GFP1–9 labelling assay (A, a, c, e, g) (0.1% BSA) and (A, b, d, f, h) (10% FBS). Higher magnification of the merge panel is illustrated. Scale bars: 10 µm. Line scans for GFP and endosomes are shown for serum starved conditions. (B) Percentage of Manders coefficient (fraction of EEA1, Rab7, LAMP1 and Rab11 positive vesicles colocalizing with RHOB/RBD). Bar graph: mean ± SEM; $n = 30$ cells from 3 independent experiments. Statistical significance between starved (0.1% BSA) and stimulated (10% serum) conditions was determined by multiple t-test using the Holm-Sidak method with alpha= 0.05 (* $P < 0.05$). The significant differences of Manders coefficient between the three compartments in selected condition (0.1% BSA or 10% serum) were evaluated by one-way ANOVA with Tukey's multiple comparisons test (##$P < 0.01$). (C) Model of RHOB/RBD complex trafficking in response to serum stimulation.

2012). The function of RHOB in the endosome could be linked to other functions. As shown by Marcos-Ramiro and colleagues in a model of endothelial cells, RHOB trafficked in an opposite manner from early to late endosomes in endothelial cell stimulated with TNF. Increase of RHOB activity using a constitutively active mutant of RHOB sequesters Rac1 in RHOB positive endosomes impeaching cell junction integrity (Marcos-Ramiro et al., 2016).

Finally, we successfully showed that tripartite split-GFP technology can be applied to the study of the localization of protein complexes involving RHO GTPases and a subset of effector proteins: PRK1, RTKN and RHPN. Our results show that although the effector binding domains of RHOA and RHOB GTPases are conserved, discrepancies are observable at the subcellular localization level. Labelling with the tripartite split-GFP assay indicate that RHOB-effectors complexes localize in the endosomes and to the plasma membrane, whereas RHOA-effectors complexes are distributed throughout the cytosol, with a slight plasma membrane localization. These differential localization of RHOA/B effectors complexes might be related to the regulation of RHOA by GDI-1, which is not the case of RHOB because of palmitoylated residues in the HVR region (Michaelson et al., 2001). The labelling of GFP11-tagged

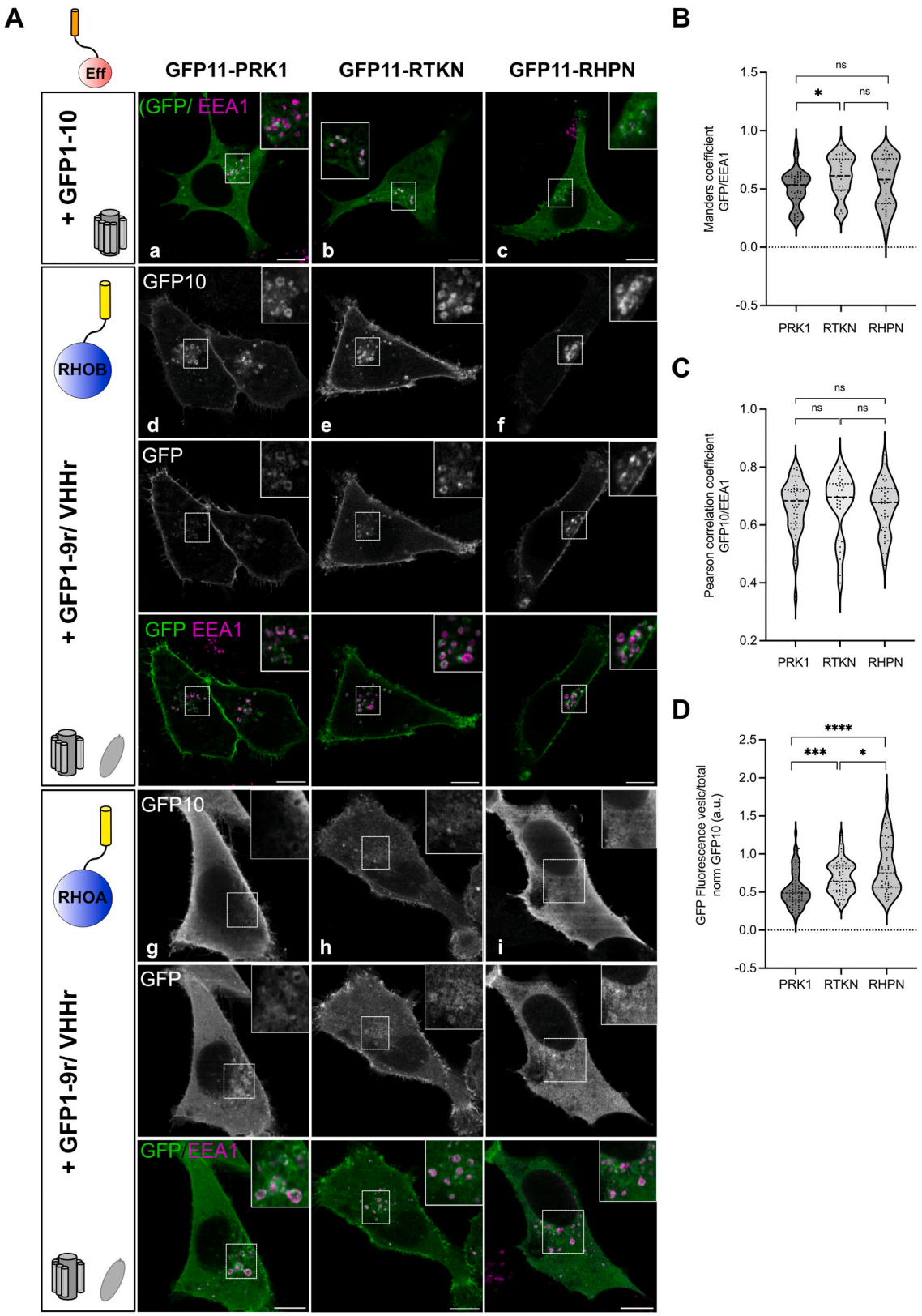

Fig. 4. Localization of RHOA/B with RHO effectors. (A) Representative micrographs of the localization of RHO effectors PRK1, rhotekin (RTKN) and rhophilin (RHPN), stably expressed in fusion with GFP11 in MRC5 cells, after transfection with the GFP1–10 moiety (a, b, c). Bottom images display the localization of RHO-effector protein complexes (GFP) and GFP10-RHO upon induction of RHOB (d,e,f) and RHOA (g,h,i) expression with doxycycline. GFP1–9r/VHHr *in vitro* labelling was applied, followed by anti-GFP10 immunostaining. Scale bars: 10 μm. (B) Violin plots: Manders coefficients for colocalization of GFP (RHOB-effector) with EEA1 positive endosomes. (C) Violin plots: Pearson coefficients for colocalization of GFP10-RHOB with EEA1 positive endosomes (D). Violin plots: quantification of vesicular/total GFP fluorescence normalized to vesicular/total GFP10-RHOB fluorescence. For B-D: n = 45 cells for PRK1, n = 35 cells for RTKN, n = 40 cells for RHPN. Student's unpaired t-test, *P < 0.05; * **P < 0.005; * ** *P < 0.001. n = 3 independent experiments.

effectors with GFP1–10 indicate a diffuse cytoplasmic localization. In contrast, several reports have shown the relocalization of PRK and RHPN to RHOB endosomes. PRK was shown, in the presence of RHOB, to relocate to endosomes (Mellor et al., 1998) where it regulates EGFR trafficking (Gampel et al., 1999). Similarly, the diffuse cytosolic Rhophilin-2 is relocalized to RHOB positive late endosomes when coexpressed with active RHOB (Steuve et al., 2006). These results point out that despite the multiplicity of interactions between RHO GTPases and their binding partners, the localization of RHO formed protein complexes will dictate the engagement of signaling accordingly.

We believe that our system has an advantage over conventional PPI detection methods to visualize the subcellular distribution of protein complexes in cells (Choi et al., 2019) because it involves small, non-perturbing split-GFP tags, and it can accommodate various protein complex conformations with the use of adequate linker lengths (Martins et al., 2023; Nonnekens et al., 2013; Polge et al., 2018; Zinzula et al., 2022). Hence, the GFP1–9 complementation *in vitro* assay does not allow live cell imaging, but enables a high-resolution imaging of protein complexes in combination with subcellular localization markers. The tripartite association requires that GFP1–9 should be expressed in excess relative to GFP10 and GFP11 fusion constructs as demonstrated using *in vitro* assays (Cabantous et al., 2013). In cells, this is achieved by either transfecting or stably expressing GFP1–9 from a strong CMV promoter or by adding recombinant protein for *in vitro* complementation. Here, in the context of small GTPase localization, inducible expression vectors were used to avoid artifacts arising from GTPase overexpression (ie RHOB). Otherwise, transient coexpression of GFP10/GFP11 fusion constructs can be readily used (as FRB/FKBP) to allow the visualization of a wide range of protein complexes.

3. Materials and methods

3.1. Cell culture and reagents

MRC5_SV (immortalized normal pulmonary human fibroblasts) cells were cultured using Dulbecco's Modified Eagle Medium (DMEM) and 10% (v/v) Fetal Bovine Serum (FBS) (Lonza, Basel, Switzerland). For cell transfection and treatments, cells were plated at a density of 20,000 cells per well of a μ-Slide 8-well ibiTreat chambered slide (Ibidi, Biovalley) for 24 h. Transfections were performed using JetPRIME® transfection reagent (PolyPlus, Illkirch, FR) with 400 ng of DNA (200 ng of each plasmid for co-transfection experiments) at 1:2 DNA:JetPRIME® ratio according to manufacturer recommendations. For 10-FRB/FKBP-11 co-transfection experiments, four hours after transfection, the medium was replaced either with fresh culture medium for untreated cells, or with cell culture medium containing 100 nM rapamycin (LC laboratories, Woburn, USA) for treated cells. For GFP1–9/ GFP VHH co-transfection experiments, cells were treated with 0.0125 μg/mL doxycycline (Sigma-Aldrich) in cell culture medium, for an additional 24 h after the transfection step.

For RHOB activation analysis, cells are washed in PBS and split-GFP reporter expression was induced for 24 h with doxycycline in serum-free DMEM medium, supplemented either with 0.1% (m/v) fatty acid-free Bovine Serum Albumin (BSA) (Sigma-Aldrich) or with 10% FBS.

For RHOB inhibition experiments with TAT-C3 peptide, the cells were treated for 24 h with cell culture medium containing 0.25 μg/mL doxycycline supplemented either with 5 μg/mL TAT-C3 peptide or 5 μg/mL TAT-β-Galactosidase control. Production of C3 exoenzyme and β-Galactosidase, coupled to permeant peptide TAT, was carried out in our laboratory following a previously described protocol (Sahai and Olson, 2006) with an additional step of size exclusion chromatography (ÄKTA Purifier FPLC system).

3.2. Plasmids and cloning

pTRIP_TRE-iBFP; pTRIP_TRE-imCherry and pTRIP_CMV-imCherry plasmids were created by inserting IRES-BFP or IRES-mCherry cassettes into pTRIP_TRE (*Xba*I:*Bam*HI) or into pTRIP_CMV (*Bam*HI:*Xho*I) lentiviral expression vectors (gifts from Loïc Van Den Berghe, Vectorology platform, Cancer Research Center of Toulouse, France).

pTRIP_TRE-GFP10-RHOB-iBFP and pTRIP_TRE-RBD-GFP11-imCherry were cloned by moving GFP10-RHOB and RBD-GFP11 DNA cassettes from pcDNA vectors (Koraïchi et al., 2018) into *Sac*II:*Xba*I cloning sites of the corresponding pTRIP_TRE vectors (Supp. Fig. 1B). The pTRIP_TRE-GFP10-RHOA-iBFP plasmid was obtained after replacing RHOB with RHOA between BspeI and *Xba*I restriction sites. Wild-type RHOA and RHOB sequences were used throughout.

Tagging full length RHO effectors with GFP11 was achieved by extending the linker sequence to 30 amino acids (GAGGSPGGGSGGSGSGGGGSGGGGSASGGS) by overlap extension PCR and cloning into a modified pDEST pTRIP_CMV-GW-imCherry vector at the N- or C-terminus of the Gateway Cassette (GW). pENTRY vectors encoding for RHPN2 (gene ID 85415) and PRK1 (gene ID 5585) were provided by the MGC platform (Montpellier, France) and pENTRY vectors encoding for NOX1 (gene ID 27035) and RTKN1 (gene ID 6242) were a gift from J.C.Twizere (GIGA, University of Liège, Belgium). Gateway LR reactions were performed to clone RTKN1, RHPN2 and PRK1 into the N-terminus GFP11 vector, and NOX1 into the C-terminus GFP11 vector.

The GFPr sequence bearing the complete split-tripartite GFP mutations (Cabantous et al., 2013) was cloned into *Nhe*I:*Xho*I sites of pcDNA_GFP1–9-CAAX (Koraïchi et al., 2018) to generate GFPr-CAAX. DNA coding for KRAS was cloned into BspeI:*Xba*I sites of pcDNA_GFP10-HRAS (Koraïchi et al., 2018). pCMV_GFP1–10 was previously described to detect GFP11-POI fusions (Cabantous et al., 2005). pcDNA_GFP10-FRB, pcDNA_FKBP-GFP11, pTRIP_CMV-GFP1–9 (Addgene# 130271) and pTRIP_CMV-GFP VHH (Addgene# 182236) constructs were previously described (Cabantous et al., 2013, Koraïchi et al., 2018).

3.3. Protein purification

Recombinant GFP1–9 expression was achieved as indicated in Martins et al., 2022, with slight modifications. The pET GFP1–9 OPT vector (Cabantous et al., 2013) (Addgene #182240) was transformed into an BL21 (DE3) *E. coli* strain and plate onto a selective Luria-Bertani (LB)-agar medium with 35 μg/mL kanamycin.

A 1 mL overnight culture was inoculated into 500 mL of LB medium containing 35 μg/mL kanamycin and was grown at 37 °C to $A_{600\,nm}$ ~0.6. The temperature was reduced to 25 °C prior to induction with 0.1 mM isopropyl β-D-thiogalactoside (IPTG) for 24 h. Bacterial cultures were collected by centrifugation at 4200 g for 10 min. Cell pellets were resuspended in 20 mL lysis buffer (150 mM NaCl, 150 mM Tris-HCl pH 7.2, 5% v/v glycerol, 0.2 mM TCEP, 10 mM imidazole) and lysed using an Emulsiflex C5 high-pressure homogenizer (Avestin). The lysate was centrifuged at 30,000 g for 20 min. GFP1–9 was extracted from the supernatant using a 1 mL of TALON® Metal Affinity Resin (Takara Bio 635503) that was equilibrated with the lysis buffer. After two washes with ten volumes of lysis buffer, recombinant GFP 1–9 was eluted with the same buffer supplemented with 200 mM imidazole. The 2-mL protein elution was then injected into a HiLoad 16/60 Superdex 75 (GE Healthcare) pre-equilibrated with 50 mM Tris-HCl pH 7.2, 150 mM NaCl, and 5% v/v glycerol (GFP1–9 SEC). Alternatively, GFP1–9 can be purified in a batch mode that include the TALON step only (referred as GFP1–9 Batch). The 200 mM imidazole eluted samples were dialyzed against 50 mM Tris-HCl pH 7.2, 150 mM NaCl, and 5% v/v glycerol buffer. Protein concentration was determined by measuring OD 280 nm and samples were kept one week at 4 °C or at − 20 °C for long term storage.

The anti-GFP VHH sequence was cloned into a pHEN6 vector that allows periplasmic expression of a carboxy-terminally fused VHH to 6xHis tag. Expression was performed in XL1 blue *E. coli* grown in Terrific

Broth (TB)-ampicillin (100 μg/mL) medium supplemented with 1% glucose in the starter culture. Expression was induced with 1 mM IPTG for 16 h at 25 °C, then cells were harvested and resuspended in 5 mL/L of ice-cold TES (200 mM Tris-HCl pH 8.0, 0.5 mM EDTA, 500 mM sucrose) supplemented with protease inhibitors and stored at − 80 °C. An osmotic shock was given by adding 15 mL/L culture of a ¼ dilution of TES buffer to the re-suspended frozen pellets prior to vortex briefly and were incubated for 30 min at 4 °C. After centrifugation (30 min, 13,000 g, 4 °C), the periplasmic extract containing GFP VHH was purified by IMAC affinity chromatography. The protein extract was incubated 2 h in the presence of Complete® His-Tag purification beads (Roche) previously equilibrated with equilibration buffer (50 mM Tris pH 8.5, 0.125 mM EDTA, 125 mM Sucrose, 1 mM $MgCl_2$, 250 mM NaCl, 10 mM Imidazole). Beads were washed with 30 mL of the same buffer before elution with elution buffer (50 mM Tris pH 7.4 – 250 mM imidazole– 500 mM NaCl) and dialysis was performed for 16 h at 4 °C in PBS 5% glycerol. OD at 280 nm was measured in order to determine protein concentration. Home purified nanobody was used for Figs. 2, 3 and 4. Recombinant Chromotek GFP nanobody was used Supp Fig. 1; and Fig. 3.

3.4. GST pulldown assays

The level of activated RhoB was performed as previously (Bery et al., 2019). Activated RhoB was measured using the GST fusion protein containing the Rho binding domain of Rhotekin (Ren and Schwartz, 2000). Cells were lysed in interaction/lysis buffer (50 mM Tris-Hcl pH7.2, 1% Triton X100, 0.1% SDS, 500 mM NaCl and 10 mM MgCl2 supplemented with protease and phosphatase inhibitors and 10 mM DTT). GST-RBD beads were incubated with cleared lysate for 40 min at 4 °C. After interaction, beads were washed with washing buffer (50 mM Tris-Hcl pH7.2, 1% Triton X100, 150 mM NaCl and 10 mM MgCl2). Beads and inputs were denaturated and separated on 12.5% SDS-PAGE Western Blot.

3.5. Generation of stable cell lines

Lentiviral vector particles for pTRIP_CMV and pTRIP_TRE vectors were produced by co-transfection with the p8.91 (Addgene #187441) and pCMV-VSV-G (Addgene #8454) packaging vectors in HEK293FT low-passage cells. Viral supernatants were harvested 48 h after tri-transfection, and filtered through 0.45 μm filter units (Millipore). For concentrated lentiviruses, an ultracentrifugation step at 24,000 rpm for 1h30 at 4 °C was performed and lentiviral vector particles were resuspended in PBS solution supplemented with MgCl2 and CaCl2 (Sigma-Aldrich). The virus preparations were aliquoted and frozen at − 80 °C.

As a general protocol for transduction, cells were plated at a density of 100,000 cells in a 12-well plate for 24 h and transduced in reduced-serum OptiMEM medium (Gibco) supplemented with 10 μg/mL polybrene (Sigma-Aldrich) at 1:1 (v/v) lentivirus: medium ratio (or 1:100 ratio for concentrated lentivirus). The medium was replaced with fresh culture medium 24 h after transduction.

The RHOB/RBD split-GFP cell model was generated by transducing MRC5 Tet-On cells (Koraïchi et al., 2018) with pTRIP_TRE-GFP10-RHOB-iBFP lentiviral vector followed by fluorescence activatedcell-sorting based on BFP fluorescence. After recovery, the cells were subsequently transduced with pTRIP_TRE-RBD-GFP11-imCherry lentiviral vector (Supp. Fig. S1). MRC5 RHOB tripartite split-GFP (triSFP) reporter cell expressing GFP VHH, GFP1–9, GFP10-RHOB and RBD-GFP11 was previously described (Koraïchi et al., 2018).

To generate stable cell lines encoding full length effectors, MRC5 Tet-On cells were transduced either with pTRIP_TRE-GFP10-RHOA-iBFP or with concentrated pTRIP_TRE-GFP10-RHOB-iBFP lentiviruses followed by a second transduction with pTRIP_CMV-imCherry encoding GFP11-tagged effectors. To achieve stable GFP1–9 expression (when indicated), the RHO effector cell models were also transduced with pTRIP_CMV-GFP1–9 (Addgene # 130271) and pTRIP_CMV-GFP VHH (Addgene #182236) lentiviruses.

3.6. GFP1-9 in vitro labelling, immunofluorescence and microscopy analysis

Ibidi chamber slides were fixed with 3.7% PFA and permeabilized with 0.1% Triton X-100 in PBS buffer. After blocking with 8% BSA in PBS, 100 μl of GFP1–9 recombinant protein (0.1 mg/mL) was added alone or supplemented with GFP VHH (0.1 mg/mL) at the indicated ratio (v/v). After determining the optimal incubation time needed, an incubation step of 4 h at room temperature was used and GFP1–9-stained cells were washed twice with PBS. For immunostaining, primary antibodies were incubated overnight at 4 °C followed by secondary antibody staining for 40 min at room temperature.

To label GFP10-tagged RHOA and RHOB, an anti-GFP10 rabbit polyclonal antibody (Agro-bio, France) and a secondary antibody PacificBlue conjugated anti-rabbit IgG (Life technologies) were used at 1:1000 dilution. To label endosomes, the following primary antibodies were used: EEA1 (Clone 14, BD Biosciences) 1:250 dilution, Rab7 (clone D95F2, Cell signaling) 1:50, LAMP1 (clone H5G11, Santa Cruz Biotechnology) 1:50, Rab11 (#5589, Cell Signaling) 1:100, followed by secondary antibody Alexa fluor 647 conjugated anti mouse or rabbit IgG (Life technologies) 1:1000. For whole cell staining, cells were incubated with HCS CellMask™ Blue staining solution (Invitrogen) according to the manufacturer recommendations.

For subcellular localization experiments, cells were imaged using LSM 880 (Zeiss, Oberkochen, Germany) confocal laser scanning microscope, using a 488 Argon laser with a 490–553 nm emission filter for GFP; Alexa 647 and DAPI labelling were acquired with Diode Pumped Solid State Lasers (DPSS) (561 nm and 405 nm), respectively using 20x and 63x/1.4 oil immersion objectives. Image analysis and fluorescence quantification on selected ROI (vesicles, whole cell) was performed with ImageJ® software. Integrated intensities were measured (integrated density=area x raw intensity) in the GFP10 and GFP ROI vesicular regions and for the whole cell fluorescence (see example **Supp** Fig. 2**D**). The vesicular/total for GFP and GFP10 intensities were defined based on the ratio of the corresponding integrated density measurements. For colocalization analysis, Manders overlap and Pearson coefficients were calculated with the JACoP plugin of ImageJ software (Bolte and Cordelieres 2006). Manders coefficient were used for colocalization of GFPr with endosomal markers to consider the difference in intensities between weaker signals of GFP fluorescence *versus* immunostaining.

In FLIP experiments, cells cultured in 0.25 μg/mL doxycycline serum-supplemented medium for 48 h were repeatedly bleached with a 100% power of the 488 nm laser (LSM 780 microscope) for 40 s every 3 min. The acquisition of 30 images was performed every minute using a 0.5% laser power with 3 frames collected prior to bleaching. The fluorescence intensity was measured in a predefined region of the plasma membrane with Zen software (Zeiss) before and after the photobleaching of an area centered on endosomes. The loss rate in fluorescence was calculated by reference to the mean of pre-bleaching fluorescence intensities that was set to 100% signal. The data were normalized to fluorescence background (area void of cells) and fluorescence intensity of the endosomes of a neighboring unbleached cell. Calculation was performed as described in Nissim-Rafinia M, Meshorer E. Photobleaching assays (FRAP & FLIP), J Vis Exp. 2011(52).

For the quantification of GFP fluorescence in FRB/FKBP and RHOB/RBD interaction experiments, cells were imaged using Operetta CLS™ High Content Analysis System (PerkinElmer) using a 20x air objective in the 488/525 nm (GFP) and 360/405 nm (cell mask) channels. To monitor the GFP fluorescence in a kinetic mode, acquisition was performed every 30 min during 6 h. Image analysis and fluorescence quantification were performed with Columbus™ analysis software. Cells were delimited, according to the CellMask blue staining, and GFP

fluorescence was subsequently quantified for each individual cell to obtain the percentage of GFP positive cells and their fluorescence intensities.

3.7. GFP1-9 in vitro complementation kinetics

10-K1/E1–11 coiled-coils were expressed from a prokaryotic bicistronic pTET SpecR tetracycline inducible vector (Cabantous et al., 2013). Protein expression was induced from a 50 mL E. coli. culture using 0.3 µg Antet (Anhydrous Tetracycline Monohydrochloride, Sigma) at 0.5 OD 600 for 5 h at 30 °C. The cell pellet was disrupted by sonication in 1 mL TNG buffer (100 mM Tris-HCl pH 7.5, 150 mM NaCl, 5% Glycerol). For quantifying the effect of GFP1–9/GFP VHH ratios, 20 µl of 10K1/E1–11 of cell extract diluted four-fold in TNG buffer was mixed with 40 µl GFP1–9 (0.1 mg/mL) and volumetric ratios of GFP VHH (0.1 mg/mL). Fluorescence kinetic (λ_{exc} = 488 nm/λ_{em} = 530 nm) was monitored with a Synergy2 fluorescence plate reader (BioTek), at 3 min intervals, for 15 h. The background fluorescence of a blank sample in the absence of 10-K1/E1–11 was measured with GFP1–9 alone or combined with the highest ratio of GFP1–9: GFP VHH (1:1).

3.8. Statistical analysis

Data analysis was performed using GraphPad Prism software. All data are presented as means ± standard error of the mean (SEM) of the indicated number of independent experiments. The statistical significance of differences between two groups was evaluated with Student's t test. For multiple two group comparisons, the Holm-Sidak method with alpha= 0.05 was applied. Multiple groups were compared using one-way analysis of variance (ANOVA) followed by Tukey's multiple comparisons test.

CRediT authorship contribution statement

Sebastian Castillo: Conceptualization, Methodology, Visualization, Writing – review & editing. **Delphine Pagan:** Investigation, Data curation, Writing – review & editing. **Rémi Gence:** Investigation, Data Curation, Writing – review & editing. **Faten Koraïchi:** Methodology, Visualization, Writing - Review & Editing. **Catherine Bouchenot:** Investigation. **Benoit J. Pons:** Investigation. **Betty Boëlle:** Investigation. **Aurélien Olichon:** Methodology, Resources. **Isabelle Lajoie-Mazenc:** Conceptualization, Methodology. **Gilles Favre:** Conceptualization, Funding acquisition. **Jean-Denis Pédelacq:** Methodology, Funding acquisition, Supervision, Writing – review & editing. **Stéphanie Cabantous:** Conceptualization, Methodology, Funding acquisition, Supervision, Writing – original draft.

Declaration of Competing Interest

The authors declare that they have no known competing financial interests or personal relationships that could have appeared to influence the work reported in this paper.

Data Availability

Data will be made available on request.

Acknowledgements

We thank L.Ligat (imaging core facility), M.Farcé (flow cytometry platform), L.Van Den Berghe and T.Fraineau (vectorology platform) for technical assistance (CRCT technology platform, Toulouse, France). This work was supported by La Ligue Contre le Cancer grant, la Fondation pour la Recherche Médicale grant [Equipe labellisée FRM (DEQ20170839117)], INSERM and an INSERM Région Midi-Pyrénées PhD fellowship for Sebastian Castillo and Faten Koraïchi. The authors declare no competing interests.

Appendix A. Supporting information

Supplementary data associated with this article can be found in the online version at doi:10.1016/j.ejcb.2023.151355.

References

Aktories, K., Wilde, C., Vogelsgesang, M., 2004. Rho-modifying C3-like ADP-ribosyltransferases. Rev. Physiol. Biochem. Pharm. 152, 1–22. https://doi.org/10.1007/s10254-004-0034-4.

Arnette, C., Frye, K., Kaverina, I., 2016. Microtubule and actin interplay drive intracellular c-Src trafficking. PloS One 11, e0148996. https://doi.org/10.1371/journal.pone.0148996.

Banaszynski, L.A., Liu, C.W., Wandless, T.J., 2005. Characterization of the FKBP.rapamycin.FRB ternary complex. J. Am. Chem. Soc. 127, 4715–4721. https://doi.org/10.1021/ja043277y.

Bishop, A.L., Hall, A., 2000. Rho GTPases and their effector proteins. Biochem. J. 348 (2), 241–255. https://doi.org/10.1042/bj3480241.

Cabantous, S., Terwilliger, T.C., Waldo, G.S., 2005. Protein tagging and detection with engineered self-assembling fragments of green fluorescent protein. Nat. Biotechnol. 23, 102–107. https://doi.org/10.1038/nbt1044.

Cabantous, S., Nguyen, H.B., Pedelacq, J.-D., Koraïchi, F., Chaudhary, A., Ganguly, K., Lockard, M.A., Favre, G., Terwilliger, T.C., Waldo, G.S., 2013. A new protein-protein interaction sensor based on tripartite split-GFP association. Sci. Rep. 3 https://doi.org/10.1038/srep02854.

Choi, S.G., Olivet, J., Cassonnet, P., Vidalain, P.-O., Luck, K., Lambourne, L., Spirohn, K., Lemmens, I., Dos Santos, M., Demeret, C., Jones, L., Rangarajan, S., Bian, W., Coutant, E.P., Janin, Y.L., van der Werf, S., Trepte, P., Wanker, E.E., De Las Rivas, J., Tavernier, J., Twizere, J.-C., Hao, T., Hill, D.E., Vidal, M., Calderwood, M.A., Jacob, Y., 2019. Maximizing binary interactome mapping with a minimal number of assays. Nat. Commun. 10, 3907. https://doi.org/10.1038/s41467-019-11809-2.

Ellenbroek, S.I.J., Collard, J.G., 2007. Rho GTPases: functions and association with cancer. Clin. Exp. Metastas-.-. 24, 657–672. https://doi.org/10.1007/s10585-007-9119-1.

Fujisawa, K., Madaule, P., Ishizaki, T., Watanabe, G., Bito, H., Saito, Y., Hall, A., Narumiya, S., 1998. Different regions of Rho determine Rho-selective binding of different classes of Rho target molecules. J. Biol. Chem. 273, 18943–18949. https://doi.org/10.1074/jbc.273.30.18943.

Gampel, A., Parker, P.J., Mellor, H., 1999. Regulation of epidermal growth factor receptor traffic by the small GTPase RhoB. Curr. Biol. 9, 955–958. https://doi.org/10.1016/S0960-9822(99)80422-9.

Gong, X., Didan, Y., Lock, J.G., Strömblad, S., 2018. KIF13A-regulated RhoB plasma membrane localization governs membrane blebbing and blebby amoeboid cell migration. EMBO J. 37, e98994 https://doi.org/10.15252/embj.201898994.

Huang, M., Duhadaway, J.B., Prendergast, G.C., Laury-Kleintop, L.D., 2007. RhoB regulates PDGFR-beta trafficking and signaling in vascular smooth muscle cells. Arterioscler. Thromb. Vasc. Biol. 27, 2597–2605. https://doi.org/10.1161/ATVBAHA.107.154211.

Huang, M., Satchell, L., Duhadaway, J.B., Prendergast, G.C., Laury-Kleintop, L.D., 2011. RhoB links PDGF signaling to cell migration by coordinating activation and localization of Cdc42 and Rac. J. Cell. Biochem. 112, 1572–1584. https://doi.org/10.1002/jcb.23069.

Kao, Y.-Y., Gianni, D., Bohl, B., Taylor, R.M., Bokoch, G.M., 2008. Identification of a conserved Rac-binding site on NADPH oxidases supports a direct GTPase regulatory mechanism. J. Biol. Chem. 283, 12736–12746. https://doi.org/10.1074/jbc.M801010200.

Keller, L., Tardy, C., Ligat, L., Le Pennec, S., Bery, N., Koraïchi, F., Chinestra, P., David, M., Gence, R., Favre, G., Cabantous, S., Olichon, A., 2022. Tripartite split-GFP assay to identify selective intracellular nanobody that suppresses GTPase RHOA subfamily downstream signaling. Front. Immunol. 13 https://doi.org/10.3389/fimmu.2022.980539.

Kirchhofer, A., Helma, J., Schmidthals, K., Frauer, C., Cui, S., Karcher, A., Pellis, M., Muyldermans, S., Casas-Delucchi, C.S., Cardoso, M.C., Leonhardt, H., Hopfner, K.-P., Rothbauer, U., 2010. Modulation of protein properties in living cells using nanobodies. Nat. Struct. Mol. Biol. 17, 133–138. https://doi.org/10.1038/nsmb.1727.

Koraïchi, F., Gence, R., Bouchenot, C., Grosjean, S., Lajoie-Mazenc, I., Favre, G., Cabantous, S., 2018. High-content tripartite split-GFP cell-based assays to screen for modulators of small GTPase activation. J. Cell Sci. 131, jcs210419 https://doi.org/10.1242/jcs.210419.

Lungu, C., Meyer, F., Hörning, M., Steudle, J., Braun, A., Noll, B., Benz, D., Fränkle, F., Schmid, S., Eisler, S.A., Olayioye, M.A., 2023. Golgi screen identifies the RhoGEF Solo as a novel regulator of RhoB and endocytic transport. Traffic Cph. Den. 24, 162–176. https://doi.org/10.1111/tra.12880.

Marcos-Ramiro, B., García-Weber, D., Barroso, S., Feito, J., Ortega, M.C., Cernuda-Morollón, E., Reglero-Real, N., Fernández-Martín, L., Durán, M.C., Alonso, M.A., Correas, I., Cox, S., Ridley, A.J., Millán, J., 2016. RhoB controls endothelial barrier recovery by inhibiting Rac1 trafficking to the cell border. J. Cell Biol. 213, 385–402. https://doi.org/10.1083/jcb.201504038.

Martins, C.S., Taveneau, C., Castro-Linares, G., Baibakov, M., Buzhinsky, N., Eroles, M., Milanović, V., Omi, S., Pedelacq, J.-D., Iv, F., Bouillard, L., Llewellyn, A., Gomes, M.,

Belhabib, M., Kuzmić, M., Verdier-Pinard, P., Lee, S., Badache, A., Kumar, S., Chandre, C., Brasselet, S., Rico, F., Rossier, O., Koenderink, G.H., Wenger, J., Cabantous, S., Mavrakis, M., 2023. Human septins organize as octamer-based filaments and mediate actin-membrane anchoring in cells. J. Cell Biol. 222, e202203016 https://doi.org/10.1083/jcb.202203016.

Mellor, H., Flynn, P., Nobes, C.D., Hall, A., Parker, P.J., 1998. PRK1 is targeted to endosomes by the small GTPase, RhoB. J. Biol. Chem. 273, 4811–4814. https://doi.org/10.1074/jbc.273.9.4811.

Michaelson, D., Silletti, J., Murphy, G., D'Eustachio, P., Rush, M., Philips, M.R., 2001. Differential localization of Rho GTPases in live cells: regulation by hypervariable regions and RhoGDI binding. J. Cell Biol. 152, 111–126. https://doi.org/10.1083/jcb.152.1.111.

Milia, J., Teyssier, F., Dalenc, F., Ader, I., Delmas, C., Pradines, A., Lajoie-Mazenc, I., Baron, R., Bonnet, J., Cohen-Jonathan, E., Favre, G., Toulas, C., 2005. Farnesylated RhoB inhibits radiation-induced mitotic cell death and controls radiation-induced centrosome overduplication. Cell Death Differ. 12, 492–501. https://doi.org/10.1038/sj.cdd.4401586.

Nissim-Rafinia, M., Meshorer, E., 2011. Photobleaching assays (FRAP & FLIP) to measure chromatin protein dynamics in living embryonic stem cells. J. Vis. Exp. JoVE 2696. https://doi.org/10.3791/2696.

Nonnekens, J., Cabantous, S., Slingerland, J., Mari, P.-O., Giglia-Mari, G., 2013. In vivo interactions of TTDA mutant proteins within TFIIH. J. Cell Sci. 126, 3278–3283. https://doi.org/10.1242/jcs.126839.

Oeste, C.L., Pinar, M., Schink, K.O., Martínez-Turrión, J., Stenmark, H., Peñalva, M.A., Pérez-Sala, D., 2014. An isoprenylation and palmitoylation motif promotes intraluminal vesicle delivery of proteins in cells from distant species. PloS One 9, e107190. https://doi.org/10.1371/journal.pone.0107190.

Pertz, O., Hodgson, L., Klemke, R.L., Hahn, K.M., 2006. Spatiotemporal dynamics of RhoA activity in migrating cells. Nature 440, 1069–1072. https://doi.org/10.1038/nature04665.

Polge, C., Cabantous, S., Deval, C., Claustre, A., Hauvette, A., Bouchenot, C., Aniort, J., Béchet, D., Combaret, L., Attaix, D., Taillandier, D., 2018. A muscle-specific MuRF1-E2 network requires stabilization of MuRF1-E2 complexes by telethonin, a newly identified substrate. J. Cachex-.-. Sarcopenia Muscle 9, 129–145. https://doi.org/10.1002/jcsm.12249.

Reid, T., Furuyashiki, T., Ishizaki, T., Watanabe, G., Watanabe, N., Fujisawa, K., Morii, N., Madaule, P., Narumiya, S., 1996. Rhotekin, a new putative target for Rho bearing homology to a serine/threonine kinase, PKN, and rhophilin in the rho-binding domain. J. Biol. Chem. 271, 13556–13560. https://doi.org/10.1074/jbc.271.23.13556.

Reinhard, N.R., van Helden, S.F., Anthony, E.C., Yin, T., Wu, Y.I., Goedhart, J., Gadella, T.W.J., Hordijk, P.L., 2016. Spatiotemporal analysis of RhoA/B/C activation in primary human endothelial cells. Sci. Rep. 6, 25502. https://doi.org/10.1038/srep25502.

Ren, X.D., Schwartz, M.A., 2000. Determination of GTP loading on Rho. Methods Enzym. 325, 264–272. https://doi.org/10.1016/s0076-6879(00)25448-7.

Ridley, A.J., 2013. RhoA, RhoB and RhoC have different roles in cancer cell migration. J. Microsc. 251, 242–249. https://doi.org/10.1111/jmi.12025.

Roberts, P.J., Mitin, N., Keller, P.J., Chenette, E.J., Madigan, J.P., Currin, R.O., Cox, A.D., Wilson, O., Kirschmeier, P., Der, C.J., 2008. Rho family GTPase modification and dependence on CAAX motif-signaled posttranslational modification *. J. Biol. Chem. 283, 25150–25163. https://doi.org/10.1074/jbc.M800882200.

Rondanino, C., Rojas, R., Ruiz, W.G., Wang, E., Hughey, R.P., Dunn, K.W., Apodaca, G., 2007. RhoB-dependent modulation of postendocytic traffic in polarized Madin-Darby canine kidney cells. Traffic Cph. Den. 8, 932–949. https://doi.org/10.1111/j.1600-0854.2007.00575.x.

Sahai, E., Olson, M.F., 2006. Purification of TAT-C3 exoenzyme. Methods Enzym. 406, 128–140. https://doi.org/10.1016/S0076-6879(06)06011-3.

Samuelsson, M., Potrzebowska, K., Lehtonen, J., Beech, J.P., Skorova, E., Uronen-Hansson, H., Svensson, L., 2017. RhoB controls the Rab11-mediated recycling and surface reappearance of LFA-1 in migrating T lymphocytes. Sci. Signal. 10, eaai8629. https://doi.org/10.1126/scisignal.aai8629.

Sandilands, E., Cans, C., Fincham, V.J., Brunton, V.G., Mellor, H., Prendergast, G.C., Norman, J.C., Superti-Furga, G., Frame, M.C., 2004. RhoB and actin polymerization coordinate Src activation with endosome-mediated delivery to the membrane. Dev. Cell 7, 855–869. https://doi.org/10.1016/j.devcel.2004.09.019.

Smithers, C., Overduin, M., 2016. Structural mechanisms and drug discovery prospects of Rho GTPases. Cells 5, 26. https://doi.org/10.3390/cells5020026.

Steuve, S., Devosse, T., Lauwers, E., Vanderwinden, J.-M., André, B., Courtoy, P.J., Pirson, I., 2006. Rhophilin-2 is targeted to late-endosomal structures of the vesicular machinery in the presence of activated RhoB. Exp. Cell Res. 312, 3981–3989. https://doi.org/10.1016/j.yexcr.2006.08.028.

Valero, R.A., Oeste, C.L., Stamatakis, K., Ramos, I., Herrera, M., Boya, P., Pérez-Sala, D., 2010. Structural determinants allowing endolysosomal sorting and degradation of endosomal GTPases. Traffic Cph. Den. 11, 1221–1233. https://doi.org/10.1111/j.1600-0854.2010.01091.x.

Vega, F.M., Colomba, A., Reymond, N., Thomas, M., Ridley, A.J., 2012. dynamics RhoB regulates cell migration through altered focal adhesion dynamics.

Wang, D.-A., Sebti, S.M., 2005. Palmitoylated cysteine 192 is required for RhoB tumor-suppressive and apoptotic activities *. J. Biol. Chem. 280, 19243–19249. https://doi.org/10.1074/jbc.M411472200.

Wehr, M.C., Rossner, M.J., 2016. Split protein biosensor assays in molecular pharmacological studies. Drug Discov. Today 21, 415–429. https://doi.org/10.1016/j.drudis.2015.11.004.

Wheeler, A.P., Ridley, A.J., 2004. Why three Rho proteins? RhoA, RhoB, RhoC, and cell motility. Exp. Cell Res. 301, 43–49. https://doi.org/10.1016/j.yexcr.2004.08.012.

Wherlock, M., Gampel, A., Futter, C., Mellor, H., 2004. Farnesyltransferase inhibitors disrupt EGF receptor traffic through modulation of the RhoB GTPase. J. Cell Sci. 117, 3221–3231. https://doi.org/10.1242/jcs.01193.

Yoshizaki, H., Ohba, Y., Kurokawa, K., Itoh, R.E., Nakamura, T., Mochizuki, N., Nagashima, K., Matsuda, M., 2003. Activity of Rho-family GTPases during cell division as visualized with FRET-based probes. J. Cell Biol. 162, 223–232. https://doi.org/10.1083/jcb.200212049.

Zinzula, L., Mereu, A.M., Orsini, M., Seeleitner, C., Bracher, A., Nagy, I., Baumeister, W., 2022. Ebola and marburg virus VP35 coiled-coil validated as antiviral target by tripartite split-GFP complementation. iScience 25, 105354. https://doi.org/10.1016/j.isci.2022.105354.